Transient-assisted plasma etching (TAPE): Concept, mechanism, and prospects

Atefeh Fathzadeh, Philippe Bezard, Maxime Darnon, Inge Manders, Thierry Conard, Ilse Hoflijk, Frederic Lazzarino, Stefan de Gendt

Transient Assisted Plasma Etching (TAPE): Concept, Mechanism and Prospects

Running Authors: Fathzadeh et al.

Atefeh Fathzadeh [1,2] , Philippe Bezard [2], Maxime Darnon [3], Inge Manders [2], Thierry Conard [2], Ilse Hoflijk [2], Frederic Lazzarino [2], Stefan de Gendt [1,2]

[1]KU Leuven, Celestijnenlaan 200f, Leuven, 3001, BELGIUM
[2]IMEC, Kapeldreef 75, Leuven, 3001, BELGIUM
[3] Laboratoire Hubert Curien, CNRS – Université Jean Monnet, F-42023, Saint-Etienne, France

[a)] Electronic mail: philippe.bezard@imec.be

Atomic layer etching (ALE) schemes are often deemed economically unviable due to their slow pace and are not suited for every material/ hard-mask combination. Conversely, plasma etching presents pattern profile challenges because of its inability to independently control ion and neutral flux. In this work, we introduce a new cyclic transient- based process, called Transient Assisted Plasma Etching (TAPE). A cycle of TAPE is a short exposure step to a sustained flow of reactant before the reactant gas injection is stopped in the second step, resulting in a plasma transient. As the plasma ignites and a substantial amount of etchant remains, a chemically driven etching process occurs, akin to conventional etching. Later in the transient, the modified surface is exposed to a reduced etchant quantity, and a sustained ion bombardment, in a similar way to ALE. The co-integration of conventional etching and Atomic Layer etching allows interesting compromises between etch control and processing time. Going for a transient plasma allows to provide the time and conditions needed for the necessary plasma-surface interactions to occur in one step. In this perspective, the mechanisms behind etch

rate, profile correction, and conservation of surface composition using amorphous carbon, as a benchmark, are discussed.

I. INTRODUCTION

The sub-nm era of semiconductor manufacturing nodes for CMOS logic will introduce many new concepts and challenges. The new generation of lithography, high-NA (numerical aperture) Extreme Ultra-Violet lithography, will not only impose constraints on photoresist thickness but will also influence the dimensions of active and sacrificial layers within the patterning stack [1]. At this scale, achieving a flat etch front becomes crucial to minimize damage to the ultra-thin layer underneath. A straight profile and minimal roughness are necessary to control the performance-defining dimensions of the patterns. An etching process with such capabilities should also be sustainable, considering resource consumption, environmental impact and throughput.

The most common plasma etching process is a continuous process based on the synergy between energetic ions with reactive neutral species from plasma [2]. The local etch rate depends on the balance between the availability and reactivity of neutral species and the energy flux provided by ions to create adsorption sites, trigger reaction, and sputter away etch by products. In an ion-limited process where the limiting parameter is the ion flux/energy, the excess of radicals can lead to lateral etching, even without significant ion involvement, albeit at a slower rate. This occurs when the reaction is spontaneous, and the byproducts are volatile. The bouncing neutral species can result in the undercutting and bowing of the etched profile [3]. This is addressed by adding passivation gases to the gas mixture, which in turn induces stress to the patterns and

increases roughness [4]. To rectify the resulting sloped profile, a dedicated over-etching step is employed, which has to also be selective towards the layer exposed beneath and provide similar profile-correcting capabilities regardless of pattern density. Nonetheless, this approach is suboptimal for materials sensitive to damage, and its limitations have been extensively examined over the past two decades[5,6] .

Atomic Layer Etching (ALE) schemes, which can be designed with minimal passivation and still ensure high-quality profiles, are becoming increasingly attractive for the thinner layers of future nodes[7,8]. Although ALE has been studied for decades worldwide, its wide adoption in high-volume manufacturing has yet to be realized, mainly due to long processing time and overall low cost-effectiveness for film thicknesses of 5 nm and above [9]. ALE separates most of the ion flux from the reactive neutral flux by splitting the etch mechanism into sequential self-limiting reactions. This time-based control enables a careful optimization of the pattern profile-defining neutral-over-ion ratio. As a result, a flat etch front can be formed and maintained for each cycle, drastically reducing the need for the problematic over-etching phase. The standard ALE approach consists of a four-step cyclic process with two half-reaction steps and two purging steps for isolating the main steps [10,11].

This paper first introduces a novel cyclic plasma etching process, TAPE, which offers significantly improved etch control over conventional plasma etching techniques, while maintaining an etch rate suitable for high-volume manufacturing. In addition, this process aims to address the case of ion-limited processes by providing more time for ions to bombard the surface before a new flux of reactive neutrals reaches the wafer's surface. To introduce and highlight the particularities of this type of process, amorphous carbon

(aC) which has a well-established etch mechanism has been chosen. The presence of both sp^2 and sp^3 hybridizations in aC, each with their distinct etching requirements [12,13], provides an opportunity to study the capabilities of this novel process to maintain surface composition without introducing additional complexity. The impact of each step is investigated in terms of etch rate, pattern morphology, and surface composition.

II. EXPERIMENTAL

In this study, 300-mm-diameter Silicon (100) wafers have been coated with 60 nm of PECVD high-density amorphous carbon, denoted as Advanced Patterning Film (APF)[14]. These blanket wafers were used to study etch rate and surface properties. Figure 1a shows Raman spectra of deposited aC film, which were deconvoluted into D and G peaks by Gaussian fitting. D and G peaks represent the vibrational motion of sp^2 carbons within the ring structure and both ring and chain structures, respectively[15]. The ratio of the D and G peaks (I_D/I_G) is linearly related to the sp^2/sp^3 hybridized ratio of aC film[16]. To study the etch profile, as shown in Figure 1b, a 10 nm-thick spin-on-glass (SOG) was used as a hard mask to pattern 60 nm-thick APF deposited on top of a 15 nm thick PECVD SiO_2. The SOG is covered by a photosensitive resist exposed to EUV photons to form 42 nm-pitch line-space patterns.

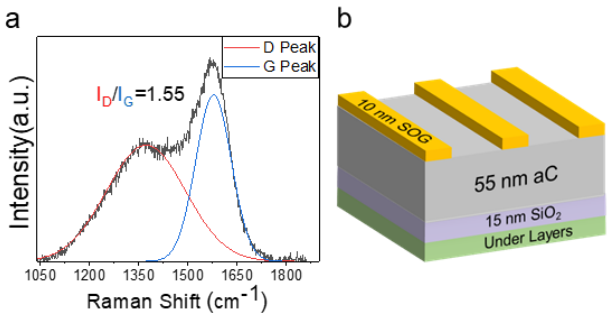

FIG. 1. (a) Raman spectra of aC film after deposition, and (b) schematic of the stack.

The experiments were performed in a Lam Research Kiyo Etcher, which is an Inductively Coupled Plasma (ICP) reactor designed to process 300 mm wafers. For all experiments, the substrate is on top of an electrostatic chuck (ESC) and is being cooled with a He backside pressure to a regulated 20ºC (no temperature mapping applied, temperature setpoint is the same for the entire wafer area). Optical Emission Spectrometer (OES) is used to detect light-emitting products during the plasma step. Characterization of oxygen density is performed by actinometry using 750 nm Ar emission peak[17].

Film thickness changes were measured ex-situ in reflection mode with a phase-modulated spectroscopic ellipsometer (KLA- Aleris) in the 300- 800 nm spectral range. A bi-layer model with a Cauchy-absorbent model with a Harmonic Oscillator model represents the silicon native oxide and the carbon blanket film. For the etch rate and the uniformity study 49 points have been measured across the wafer, and the thicknesses are averaged by area defined by five different radii (0; 4.5; 9 and 14 cm).

Scanning Electron Microscopy (SEM) and Transmission Electron Microscopy (TEM) have been used to assess the morphological impact (undercut, bowing, footing, etc.) of the different etching conditions on patterned wafers. Electron energy loss spectroscopy (EELS) has been used for localized chemical analysis of the patterned samples. X-ray Photoelectron Spectroscopy (XPS) has been used to study the surface composition after partial plasma etching. The measurements were carried out in Angle Integrated mode using a QUANTES instrument from Physical electronics. A monochromatized photon beam of 1486.6 eV with a 100-micron-wide spot was used with charge neutralization active during the measurement; all data presented are for the 45-degree exit angle. Horiba

Jobin-Yvon HR800 Raman Spectroscopy tool with 532 nm laser with 25% ND filter has been used for film characterization. The surface roughness of the aC thin films was observed by atomic force microscopy (AFM).

The chamber walls were cleaned and SiO-coated following the process conditions proposed by Ramos *et al* to maintain stable chamber conditions [18]. The process's reproducibility was assessed by executing the same procedure on five wafers, and the outcomes were collectively considered for error evaluation.

Moreover, when dealing with patterned samples, additional plasma steps are necessary to transfer the patterns from the photoresist into the spin-on-glass (SOG) layer (using CF_4-based plasma chemistry) and to strip the metal-containing photoresist (using HBr). These steps were consistently applied before each experiment (including experiments on amorphous carbon blanket wafers) to account for their potential effects on the surface of amorphous carbon and the final etch rate.

III. RESULTS AND DISCUSSION

A. Transient Assisted Plasma: Concept

The transient-assisted plasma process is a cyclic process, involving at least two steps: the injection of reactant and its termination, leading to a plasma transient phase characterized by the decay of reactant concentration. It is worth mentioning that this process can be used both in the etching and deposition process. In this article, we aimed to discuss the etching application called Transient Assisted Plasma Etching. This design provides more control over the dose of reactive species in addition to providing the necessary ions for ion-limited etching process due to the increasing ion-to-neutral ratio over plasma time.

Hence, early during the plasma step, a chemically-driven etching process occurs when a substantial amount of etchant is present. The modified surface/profile will then be exposed to a reduced etchant quantity and a continued ion bombardment. Depending on requirements, additional steps or gases can be introduced for specific purposes, making this type of process flow suitable for a wide range of reactants and materials for several important applications.

A defining aspect of TAPE is reliance on a gas transient during plasma, which is characterized by the flow of the reactive gas, its residence time (lost either by pump down or consumption) and the species outgassing from all surfaces in the chamber. The contribution of pump down is determined by the total gas flow, and the opening ratio of the pendulum valve, which regulates pressure by adjusting the effective pumping rate. Assuming a constant gas temperature (300K), pressure, and a gas flow coming only from gas injection, one can determine the residence time as:

$$\tau \approx 0.08.\frac{V.P}{Q}$$

With τ the residence time in seconds, V the volume of the chamber (in L), P the chamber pressure (in mTorr) and Q the injected gas flow (in sccm).

In addition to the pumping rate, for each cycle, some molecules/atoms are adsorbed onto the entire surface of the reactor and released during the plasma step. This outgassing allows here a more thorough usage of injected gas compared to other processes where the injection is sustained. The decay time is therefore controlled both by the residence time in the plasma and the lifetime of surface-adsorbed species on the reactor walls.

B. aC TAPE: a case study

To simplify the demonstration of this new process flow, amorphous carbon has been selected for its sp^2 and sp^3 hybridization and etchability with only a single reactant gas. Given that sp^3 carbon needs more chemical species to be etched while sp^2 carbon needs more ions[12,13], aC is a good candidate to show the impact of increasing ion-to-neutral ratio over the plasma time on the surface composition.

Figure 2a illustrates the two steps of TAPE in this context: (1) a reactive gas exposure step (no plasma) by injecting O_2 diluted in Ar, and (2) a plasma step by cutting the injection of O_2, without any purge step in between. The default conditions used for all measurements were 200 sccm of Ar and 10 sccm of O_2 (~5%O_2) at 10 mTorr pressure in the gas phase. Injection of O_2 is intentionally stopped as soon as the plasma is ignited by applying 300 W source power, and a bias voltage (DC component of the polarization of the ESC by RF bias power) regulated at 60 V, with the same Ar gas flow and pressure as during the gas step. Henceforth, all shown results follow the mentioned condition unless otherwise specified. Figure 2b shows the linear correlation between etch depth and number of cycles indicative of the reproducibility of the etch cycles of TAPE. Figure 2c shows TEM micrograph of aC after 30 cycles of TAPE, showing a straight etch profile and flat etch front, without adding other gas for passivation purpose.

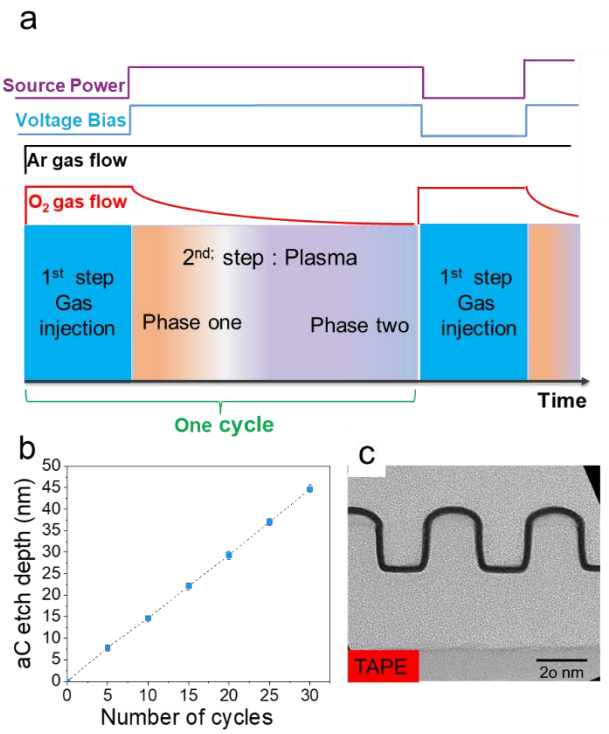

FIG. 2. (a) schematic of the TAPE process, (b) etch depth evolution with the number of cycles, (c) TEM micrograph of the etched aC sample with 30 cycles of TAPE (with 4s-long plasma steps).

In the case of etching aC with oxygen in the mentioned conditions, the residence time using eq 1 is shorter than 500 ms, meaning almost all of the O_2 molecules should be pumped out within less than a second. To verify this time scale, we looked at the dynamic evolution of the O_2 molecule concentration at the beginning of the plasma step time using actinometry. Optical Emission Spectroscopy (OES)-based actinometry has been used to follow the evolution of O_2 concentration. To this end, the intensity of the 777 nm wavelength corresponding to atomic oxygen resulting from dissociative excitation[19] is divided by the intensity of the 750 nm wavelength from excited Ar atom. The measurement of the two intensities was performed with two different gains for the OES CCD to avoid saturation. The (dissociative) excitation cross-section having a similar shape and threshold energy[20], the effect of the evolution of the electron temperature and density on the 777 nm intensity will be cancelled out by similar evolution of the Ar 750 nm intensity[21]. In this calculation, we neglect the direct excitation of O radicals which is known to be lower than the dissociation of oxygen, especially at low O_2

concentrations[19]]. Figures 3a and 3b show that the density of oxygen in the plasma decays within approximately 4 seconds after stopping the injection and starting the plasma. This significantly longer decay time than residence time calculation is due to outgassing of O/O_2 from the chamber walls and the wafer. A change of slope in the O signal during the first second is observed, most likely due to valve movements.

The plasma step is divided into three phases. Phase one (two first seconds in our configuration), where the atomic oxygen concentration is high, is suspected to exhibit similar etching mechanisms as in conventional plasma etching. Phase two has a much lower oxygen density and etching mechanisms closer to an Atomic Layer Etching process are suspected, *i.e.*, an Ar plasma on an O-covered surface. The third phase corresponds to a constant, extremely low reactant flow, close to pure argon sputtering and offering little benefit. It should be noted that there are always O_2 molecules in the chamber due to residual pressure / air leaks for instance (0.5 mTorr at the time of the measurement), which is why the background flow of O radicals does not go down to zero in OES data (crosshatch area in Figure 3a). In the TAPE process, the plasma step time is set to include only the first two phases.

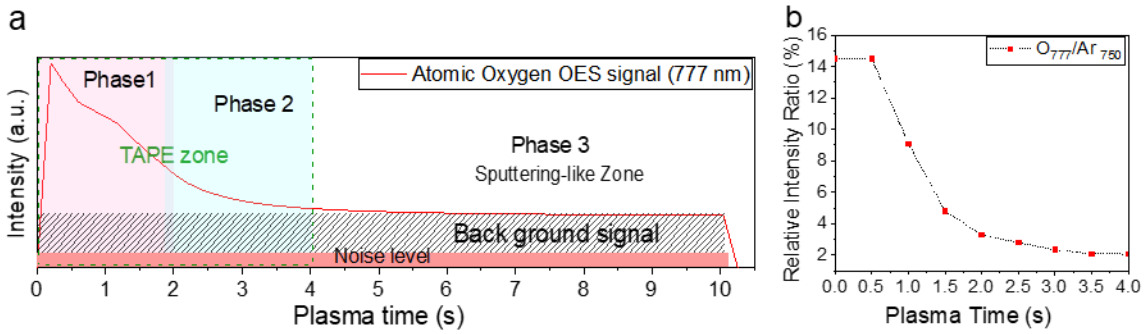

FIG. 3. (a) atomic oxygen OES signal in the plasma step of one cycle of TAPE, and (b) relative intensity ratio of atomic oxygen (I_{777}/I_{750}) in one cycle (4s) of TAPE.

C. Mechanisms: Gas exposure step

The exploration of the etching mechanism begins by examining how the gas exposure step influences the surface and its role in determining the etch rate on patterned

wafers. Once this aspect is clarified, the conditions in the gas step will remain constant, and attention will shift to the plasma step.

To understand the function of the gas exposure step within the process and its duration, the impact of gas exposure on the composition of the surface, the etch rate, and the profile are investigated. The probability of O_2 molecule adsorption is maximized on the surface bombarded by ion, therefore the surfaces of two samples processed by 20 cycles of TAPE with and without a final 6-second-long exposure to O_2 gas were compared in Figure 4a. The results show no discernible change in the atomic concentration even if the surface was first exposed to several cycles of etching.

Any contribution from physisorption that was not detected by XPS has been assessed by comparison of two samples etched with different gas exposure step duration (1 and 6 seconds). SEM results (Figure 4b) show no significant difference in etched thickness and etch profile. Most benefits in terms of etch rate or profile from the gas-exposure step are already reached with 1 second of the gas step. Therefore, we can conclude that the primary function of this step is to fill up the chamber with reactant gas which is already fulfilled within 1s. Extending this gas step has no impact. Consequently, a 1-second gas-exposure duration will be used as the first step in a cycle for every following experiment.

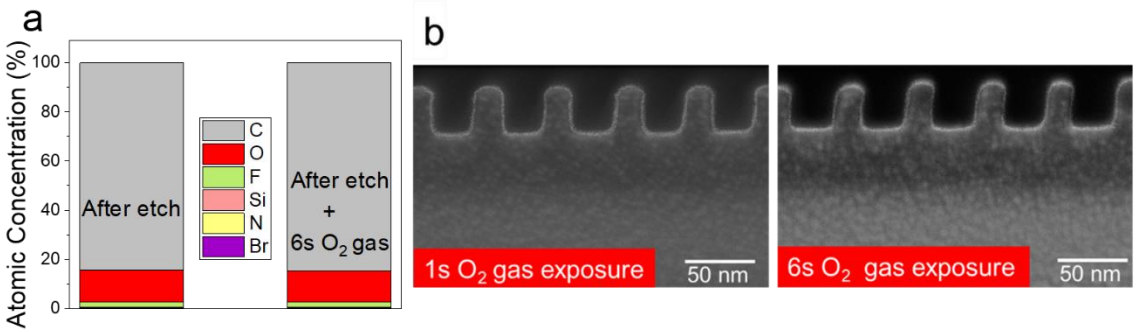

FIG. 4. (a) XPS measurement of atomic concentration of aC surface after 20 cycles of TAPE and after 20 cycles of TAPE followed by 6s gas exposure, and (b) cross-sectional SEM micrographs after 30 cycles of TAPE with 1- and 6-second-long gas steps.

D. Mechanisms: Plasma transient step

In this section, insights into the mechanisms involved in the complex plasma transient step are obtained by assessing the impact of the plasma step duration on the surface composition, etch depth, and etching profile. The etched depth and etch profile as a function of plasma step duration for a 30-cycle process are shown in Figures 5a and 5b. Plasma duration below 2s (phase one) leads to excessive footing while extending it beyond (phases one and two) allows rectifying footing and obtaining a straighter profile with a flat etch front, while the etched depth drops to less than 0.15 nm per cycle. The black line in Figure 5a represents the measured etch depth with an Ar plasma by physical sputtering using the conditions of step 2 and 0 sccm O_2 injected in step 1 (only oxygen from the residual pressure is present). This etch rate corresponds to the one observed during phase three. Figure 5c shows the overall etch rate as a function of plasma duration in each cycle.

Figure 5d shows the results of using plasma instead of gas phase during the injection. A continuous Ar/O_2 plasma has been ignited and the oxygen supply has been cut off after 1s, creating the desired plasma transient. Having plasma in the first step results in pronounced bowing and undercutting requiring longer correction times. Yet the final profile would not be as straight as the result of the process with gas in the first step.

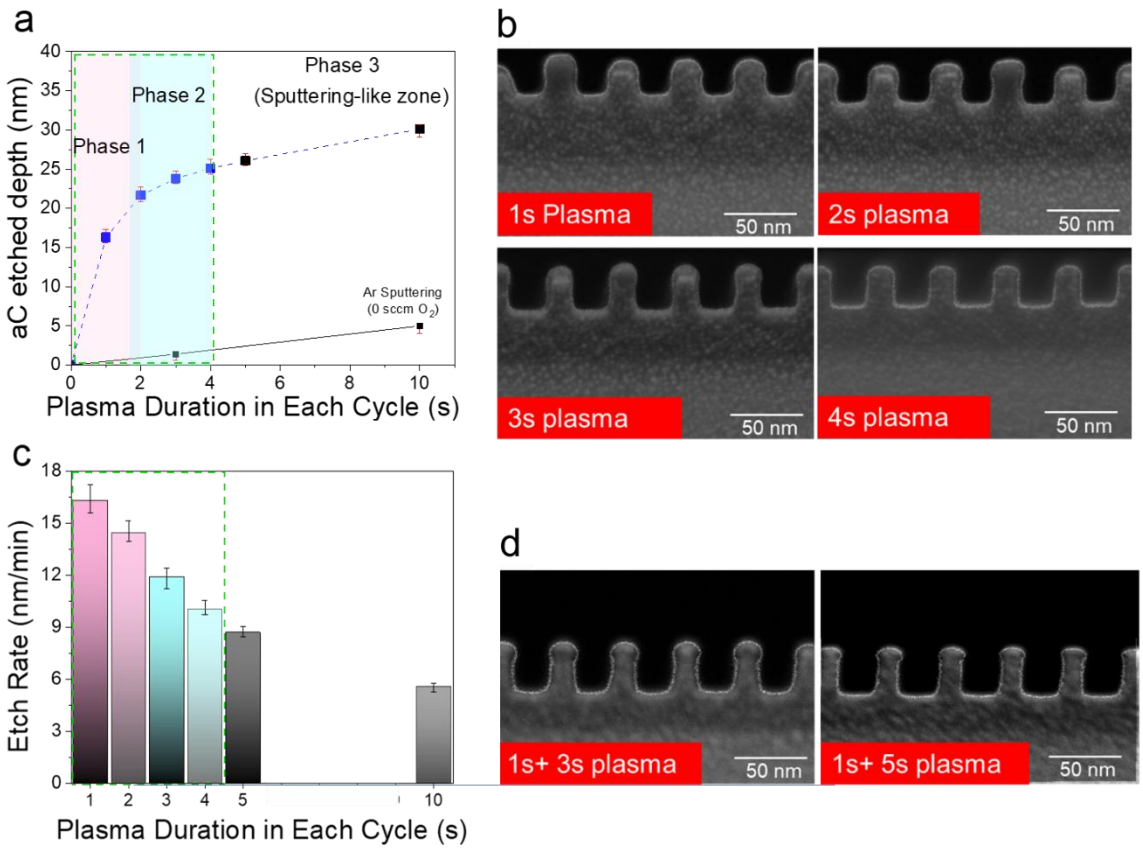

FIG. 5. (a) Etched depth as a function of plasma step duration for a 30-cycle process, (b) Cross-sectional SEM Images after 30 cycles of TAPE (1s-long gas step followed by 1 to 4 s-long plasma step), (c) Etch rate evolution as a function of plasma time, and (d) SEM image of samples after 30 cycles of TAPE with a 1s-long plasma-based first step and 3 and 5 second-long second step.

The impacts of etch conditions on instantaneous etch rate were studied in order to identify how variations in plasma parameters influence the etch rate and the etch-rate-limiting species in each phase. Figure 6a shows that for a 1s process, the instantaneous etch amount doesn't monotonously depend on pressure. If the etching rate was limited by the availability of O atoms it would increase rapidly with pressure which is not the case. Hence, it can be concluded that under this condition, ions are the limiting factor for the etch rate in the first phase. In the second phase, however, the largest etch rate is observed

at higher pressure, indicating a neutral-limited process. Figure 6b shows that while doubling the RF source power from 150 to 300 W results in a doubling in the etch rate, large diminishing returns are observed when further doubling the power from 300 to 600 W. This quasi saturation of the etch rate could indicate a transition from ion- to neutral-limited reactions. Therefore, the evolution of the etch rate as a function of pressure has been measured at both 300 and 600 W. Figure 6c shows that at 600 W, the etch rate monotonously increases with pressure from 5 to 20 mTorr, now indicating a neutral-limited process after only 1 second of plasma. Increasing the RF source power can thus accelerate the transition between the two etch regimes. Figure 6d shows that O_2 concentration in the gas mixture increases the etch rate as well up to a certain point which is due to the change in ion to neutral flux ratio[22–25].

Figure 6e shows the etch depth non-uniformity after 30 cycles of 1, 4 and 10 second-long plasma steps at 300 W source power compared to 60 seconds of conventional etching. For 10s-long plasma TAPE, the etch regime is extremely limited by neutral (sputtering-like regime in most areas), and the largest etch rate is observed at the wafer's edges, most likely due to the presence of oxygen provided by air leaks (residual pressure, as shown and discussed in figure 3a). Moving from ion limited to neutral limited regime, the etch rate at the center decreases while the etch rate at the edge increases, leading to compensation in etch depth uniformity across the wafer. This time-dependent ion-to-neutral ratio in TAPE provides better uniformity compared to the conventional etching. It is recommended to configure phase one as ion-limited to allow a transition from an ion-limited to a neutral-limited regime if achieving precise profile control is the primary concern.

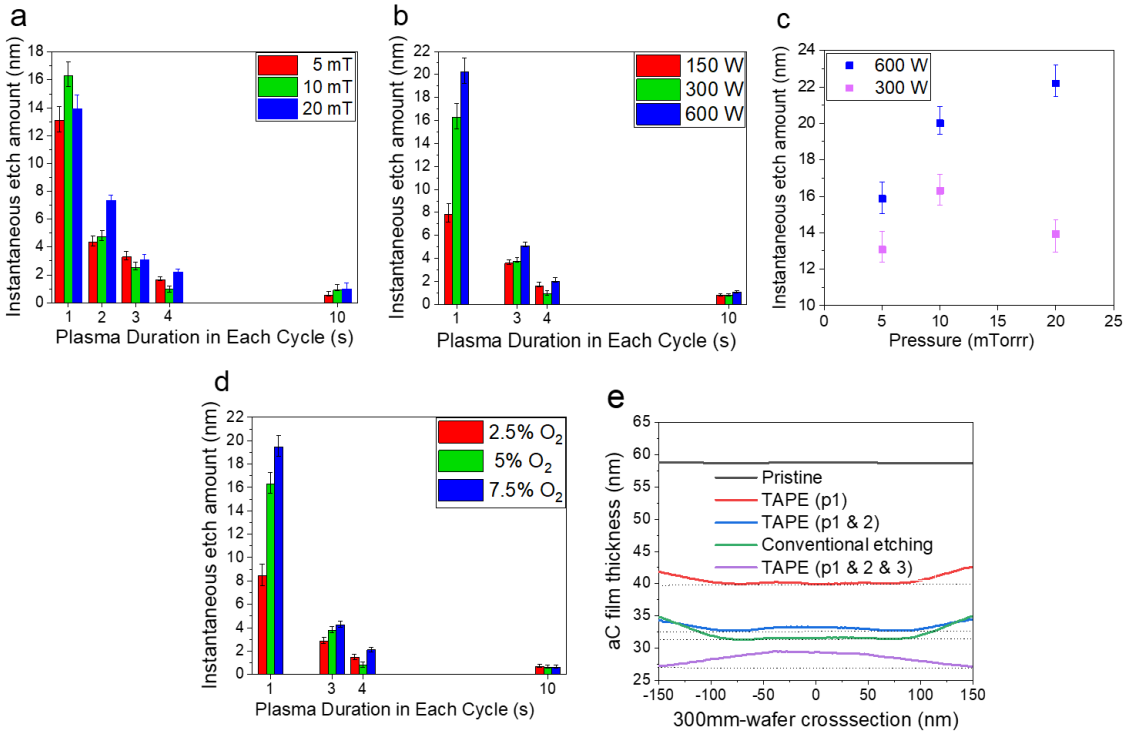

FIG. 6. Time evolution of the instantaneous etch rate as a function of (a) pressure, (b) RF source power, (c) oxygen partial pressure, (d) Instantaneous etch rate as a function of pressure after 1s-long plasma for 300 W and 600 W RF source powers, and (e) film thickness uniformity across the 300 mm wafer after etching.

E. Plasma and surface interaction

Given the dynamic nature of the process, it is necessary to examine how the interaction between the plasma and the surface evolves during the etching process. Figure 7a shows the Oxygen elemental concentration measured by XPS at the aC surface after 20 cycles of TAPE with different plasma times (1.5, 3, and 4 seconds) and conventional plasma etching. In comparison to the pristine material, samples subjected to plasma etching and TAPE with 1.5s-long plasma exhibit larger oxygen concentrations than the pristine material. However, for longer plasma step durations, there is a decrease in the oxygen concentration, returning it closer to its initial level.

Figure 7b shows deconvoluted C1s spectra after 20 cycles of TAPE for samples with 1 to 4s-long plasma steps by using the CA(C,H) component of the C1s peak set at 284.8 eV as the reference for the BE scale. The peaks at 284.6 and 285.2 represent sp^2 and sp^3 carbon, the peak at 286.3 eV represents alkoxy groups (C–O), and the peak at 287.7 eV represents carbonyl groups (C=O), and the peak at 289.2 eV represents carboxylate group (O-C=O) [15,26,27]. Deconvoluted peaks have excellent agreement with the measured D-parameter and Raman in terms of sp^2 and sp^3 ratio for this sample.

A significant increase in the population of O-C=O bonds is observed in phase one (~ 0-2s), while during the second phase, it returns to the original amount, as shown in Figure 7c. The creation rate of O-C=O bonds, related to the amount of oxygen in the chamber, decreases over time (as well as the removal of the oxidized layer), while their destruction rate, related to the ion flux, increases over time. Therefore, in the first phase, more O-C=O bonds are formed than etched till the ion-to-neutral flux ratio becomes high enough to consume what has been previously created. The D-parameter, obtained from the X-ray-induced C-KLL Auger peak, where depending upon the relative concentrations of sp^2 and sp^3 carbon, the separation of the differential (D, hence D-parameter) maxima and minima differ greatly and hence it is used to extract the relative amounts of sp^2 and sp^3 carbon at the surface (<10 nm deep)[28]. Figure 7d shows a reduction in the D parameter following both the first phase (2s-long plasma) and conventional etching compared to the pristine film. Meanwhile, for (4s-long plasma) TAPE sample it subsequently reverts to its original value. Given that a smaller D parameter corresponds to a higher concentration of sp^2 carbon, results show sp^2/sp^3 increase in the first phase. This implies that there is a preference for the consumption of sp^3-carbon during this phase. However, during the

second phase, the sp^2-rich carbon layer is sputtered away, recovering a sp^2/sp^3 ratio close to the pristine film. The variation of the sp^2/sp^3 has been considered in the deconvolution of the C1s peaks. The same trend is observed for surface roughness for the samples etched by TAPE (2s and 4s long plasma) and the conventional etching, shown in Figure 7e. The structure of hydrogenated amorphous carbon films may be pictured as sp^2-carbon atoms in condensed aromatic clusters, dispersed in an sp^3-rich matrix [29,30].During the first seconds, the plasma mostly etches the sp^3 carbon, and these sp^2 clusters are revealed and make the surface appear rough. By extending the plasma time to etch these sp^2 clusters, the surface gets smoothened.

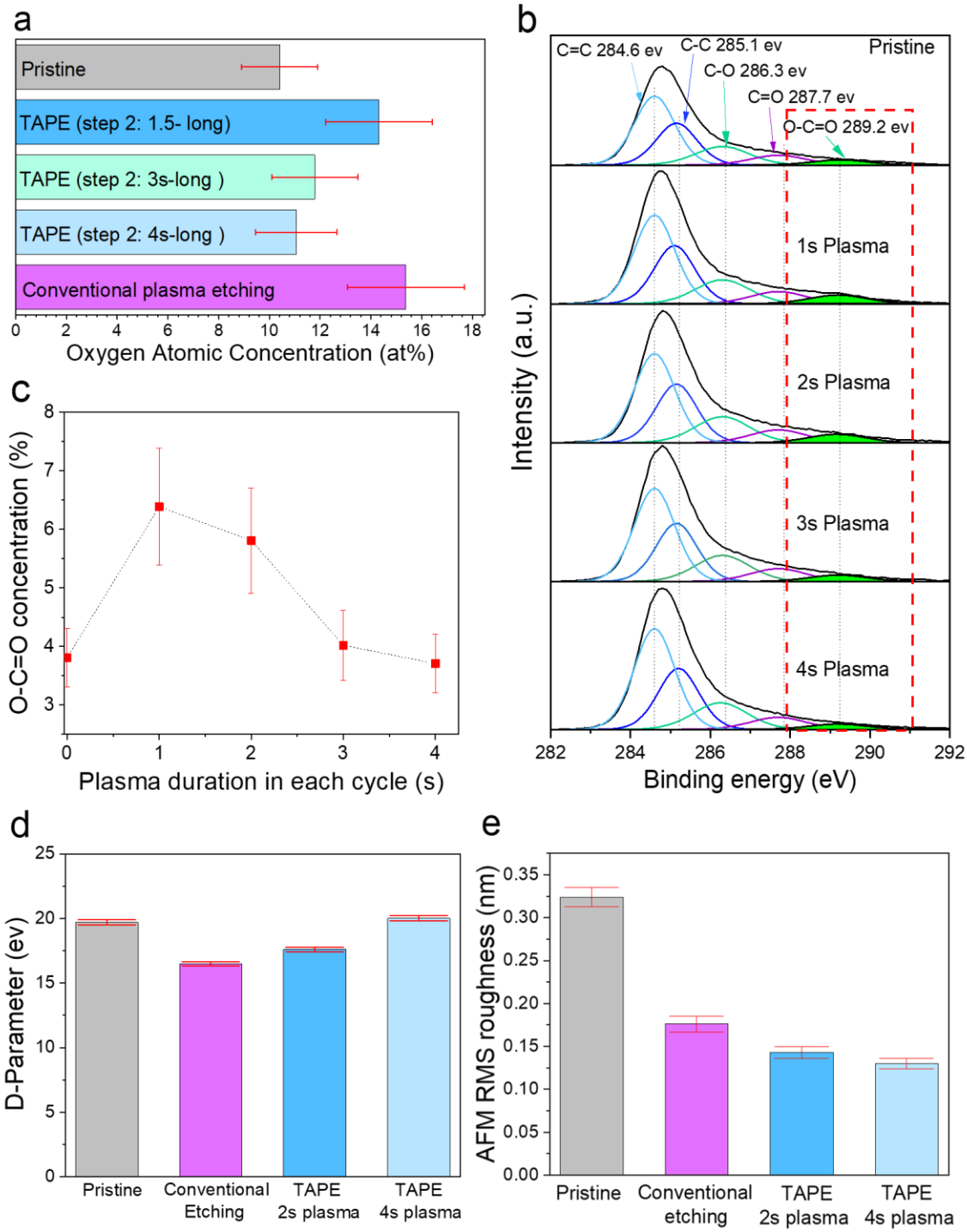

FIG. 7. (a) Oxygen atomic measured by XPS after exposure to the different etch processes condition, (b) C1s peak deconvolution from the aC surface after 20 cycles of TAPE with 1 to 4 s-long plasma steps, (c) O-C=O bonds concentration as a function of plasma time (1-4s), (d) D-parameter of aC surface before and after etching with TAPE (2 and 4 s-long

plasma step), and (e) Root-mean-squared (RMS) surface roughness of aC surface before and after etching with TAPE (2 and 4 s-long plasma step).

F. Profile study

In this section, the contribution of both phase one and phase two is addressed, exploring their effects on the profile while considering various plasma and process parameters. As previously discussed, the ion-limited nature of the first phase increases the oxygen concentration on the surface mainly as O-C=O bonds. These bonds should persist longer in regions where insufficient ions can reach, i.e., at the bottom of the trench and specifically where footing is observed in Figure 8a. Figure 8b shows the evolution of carbon over oxygen ratio of the bottom of the trench in patterned samples after 30 cycles of TAPE with different plasma durations (1 to 4s), characterized by EELS. This is consistent with the finding of Cunge et al.[31], who showed that the loss of ion flux between the top and bottom of a high aspect ratio structure is dominated by the ion angular distribution and geometric shadowing. Therefore, the ion fluence provided by this extra plasma time allows hardly accessible chemisorbed oxygen atoms during the first phase to finally react and desorb as CO_x[32,33]

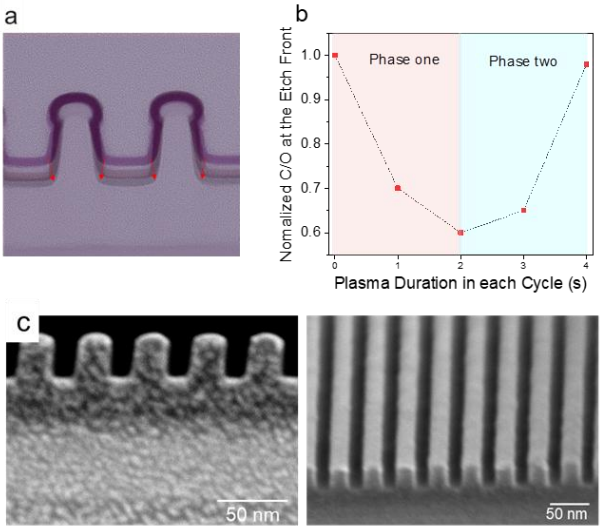

FIG. 8. (a) superposed TEM micrograph after 30 cycles of 1s-long gas step followed by 1 to 3s-long plasma step, (b) Evolution of C/O ratio at the etch front based on EELS characterization, and (c) Cross-sectional SEM after 7.5 % O_2 in the gas step with 300 W of source power, 90 V bias voltage in the first phase, and 200 W of source power, 60 V bias voltage in phase two.

Since the TAPE relies on a gas transient, there is a transition from ion to neutral limited regime, not existing in conventional plasma etching. Therefore, there is a possibility to optimize each phase to reach a better trade-off between the etch rate, profile, and selectivity to the hard mask. Providing larger oxygen ion flux with higher ion energy (E_i) within phase one and lower ion flux (Γ_i) with medium ion energy (E_i) within phase two increases the etch rate while maintaining the desired etch profile and selectivity to the hard mask. The higher ion energy (E_i) in phase one is required to minimize ion deviation and provide enough passivation through sputtered SOG to minimize undercut and bowing [34]. The medium ion energy (E_i) in the second phase is required to ensure the ions possess enough energy to reach the pattern's bottom corners. A SEM image (Figure 8c) of a sample etched under these specified conditions demonstrates an improvement in the etch

rate, increasing from 10.1 nm/min as shown in Figure 2b and 5a (~ 0.8 nm Etch Per Cycle (EPC)) to 17 nm/min (~ 1.1 nm EPC), while maintaining the desired etch profile and selectivity to the hard mask.

IV. CONCLUSIONS AND PROSPECTS

A novel cyclic etching process, referred to as Transient Assisted Plasma Etching (TAPE), has been introduced. The process involves at least two steps: the injection of reactant and its termination, leading to a plasma transient phase characterized by the decay of reactant concentration. The concept of the process and the purpose of the design were discussed by using aC as a case study material. It was shown this approach yields a notably improved etch profile compared to traditional plasma etching and offers superior etch rates compared to conventional in the absence of external passivation for amorphous carbon.

The plasma step can be decomposed into phases. When most etchant species are still present in the chamber (phase one), the process is limited by the ion flux, and in the case of aC many O-C=O bonds are formed, especially at the corner of the patterns where ion flux is reduced by ion shadowing effects. When most etchant species have been pumped out or consumed and plasma primarily consists of Ar atoms (phase 2), the process is limited by the presence of chemical species coming from the gas phase or adsorbed at the surface. The O-C=O bonds that remained in the bottom corners of patterns provide the necessary reactants to form volatile products, which corrects the etch profile. Due to the overall lack of reactive neutrals in the etch chamber during this phase, the etch rate is limited by neutral species, and no extra passivation layers are needed to protect the sidewalls. Figure 9 summarizes the etching trend of the TAPE process for aC, A trade-off

has been observed between etch rate, profile control, and selectivity with the hard mask. It has then been shown that it can be improved by providing suitable ion flux/ energy and energy flow for each phase.

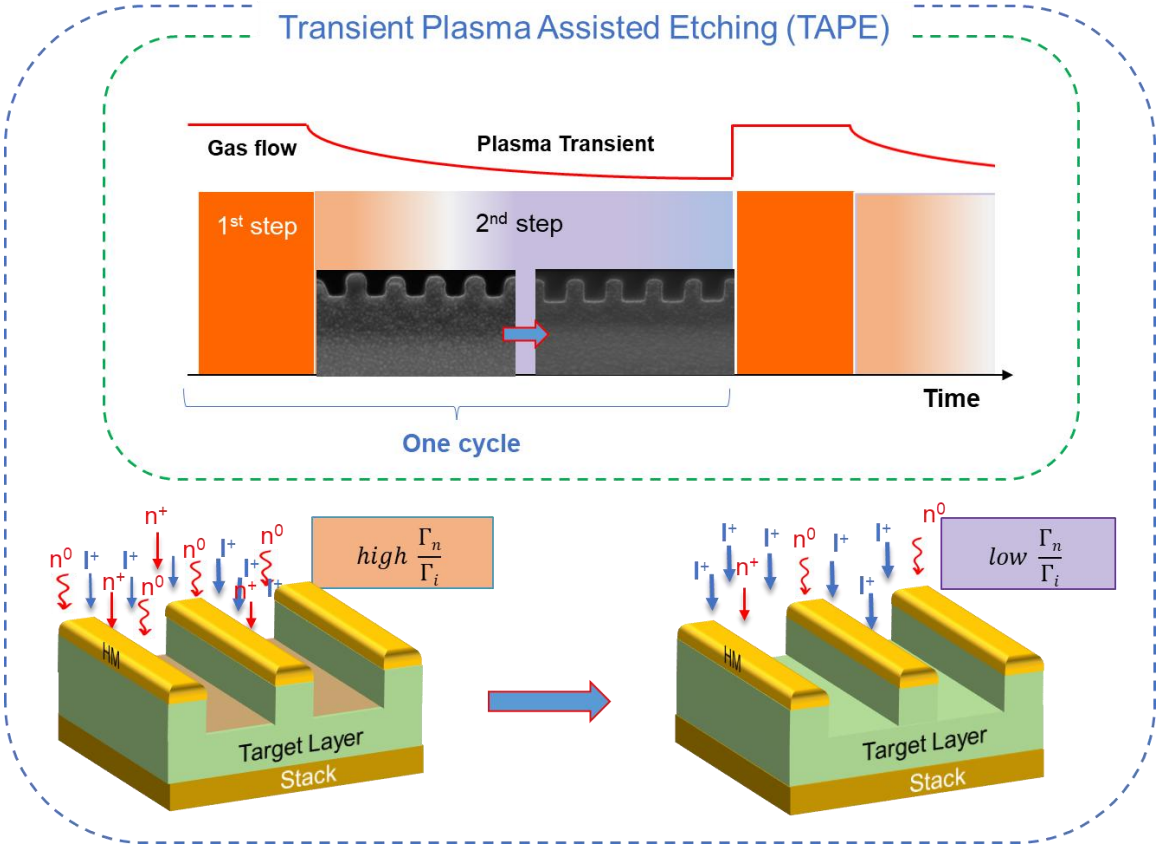

FIG. 9. Schematic illustration of the etching trend of the general TAPE process.

The concept proposed here and demonstrated for amorphous carbon etching by an oxygen-based process can be extended and applied to other materials with other reactive and inert gases regarding the material and concerns. We believe it is particularly well suited for mask patterning, alternative metals etching for first levels of interconnects, residue removal from sensitive material, descum of ultra-thin photoresist, and dielectrics etching (contact and vias). In this article, we demonstrate compositional drift like the sp^2/sp^3 ratio could be corrected. This property positions the TAPE process as a promising

choice for etching compound materials (alloys, materials containing diverse elements, etc.). Moreover, its design combines some of the pattern control capabilities of Atomic Layer Etching with etch rates that are compatible with high-volume manufacturing, akin to conventional plasma etching. Consequently, it is suitable for nano-scale patterning while offering precise profile control for layers that exceed the thickness limitations of ALE (greater than 10nm). Finally, this process is not only fully compatible with area-selective deposition processes, but also can be employed for the deposition itself to control the composition of the deposited films.

AUTHOR DECLARATIONS

Conflicts of Interest *(required)*

The authors have no conflicts to disclose.

DATA AVAILABILITY

The data that supports the findings of this study are available within the article and its supplementary material.

REFERENCES

[1] https://www.asml.com/en/news/press-releases/2006/asml-presents-leading-edge-immersion-results

[2] J.W. Coburn, and H.F. Winters, J. Vac. Sci. Technol. **16**(2), 391–403 (1979).

[3] K. Ishikawa, T. Ishijima, T. Shirafuji, S. Armini, E. Despiau-Pujo, R.A. Gottscho, K.J. Kanarik, G.J. Leusink, N. Marchack, T. Murayama, Y. Morikawa,

G.S. Oehrlein, S. Park, H. Hayashi, and K. Kinoshita, Jpn J Appl Phys **58**(SE), SE0801 (2019), https://doi.org/10.7567/1347-4065/ab163e .

[4] G.S. Oehrlein, R.J. Phaneuf, and D.B. Graves, J. Vac. Sci. Technol. B **29**(1), 010801 (2011), https://doi.org/10.1116/1.3532949 .

[5] P. Brichon, E. Despiau-Pujo, and O. Joubert, J. Vac. Sci. Technol. A **32**(2), 021301 (2014), https://doi.org/10.1116/1.4827016 .

[6] C. Petit-Etienne, M. Darnon, P. Bodart, M. Fouchier, G. Cunge, E. Pargon, L. Vallier, O. Joubert, and S. Banna, J. Vac. Sci. Technol. B **31**(1), 011201 (2013), https://doi.org/10.1116/1.3622311

[7] M. Honda, T. Katsunuma, M. Tabata, A. Tsuji, T. Oishi, T. Hisamatsu, S. Ogawa, and Y. Kihara, J Phys D Appl Phys **50** 234002, (2017), DOI 10.1088/1361-6463/aa6f27.

[8] K.J. Kanarik, T. Lill, E.A. Hudson, S. Sriraman, S. Tan, J. Marks, V. Vahedi, and R.A. Gottscho, J. Vac. Sci. Technol. A **33** 020802, (2015), https://doi.org/10.1116/1.4913379 .

[9] K.J. Kanarik, S. Tan, W. Yang, T. Kim, T. Lill, A. Kabansky, E.A. Hudson, T. Ohba, K. Nojiri, J. Yu, R. Wise, I.L. Berry, Y. Pan, J. Marks, and R.A. Gottscho, J. Vac. Sci. Technol. A **35,** 05C302, (2017), https://doi.org/10.1116/1.4979019 .

[10] K.J. Kanarik, S. Tan, and R.A. Gottscho, J Phys Chem Lett **9**(16), 4814–4821 (2018), https://doi.org/10.1021/acs.jpclett.8b00997.

[11] G.S. Oehrlein, D. Metzler, and C. Li, ECS J. Solid State Sc. **4**(6), N5041–N5053 (2015), DOI: 10.1149/2.0061506jss.

[12] J. Li, S.J. Kim, S. Han, Y. Kim, and H. Chae, Plasma Process Polym. **18**(11), (2021), https://doi.org/10.1002/ppap.202100075

[13] A. Davydova, E. Despiau-Pujo, G. Cunge, and D.B. Graves, J. Phys. D Appl. Phys. **48**(19), 195202 (2015), DOI: 10.1088/0022-3727/48/19/195202

[14] H. Tai, Y.-M. Liao, W.-T. Liu, W.-C. Peng, and T.-H. Ying, ECS Trans. **61**(3), 67–71 (2014).

[15] F.C. Tai, S.C. Lee, C.H. Wei, and S.L. Tyan, Mater. Trans. **47**(7), 1847–1852 (2006), https://doi.org/10.2320/matertrans.47.1847.

[16] J. Li, S.J. Kim, S. Han, and H. Chae, Surf. Coat. Technol. **422**, 127514 (2021), https://doi.org/10.1016/j.surfcoat.2021.127514 .

[17] D. V Lopaev, A. V Volynets, S.M. Zyryanov, A.I. Zotovich, and A.T. Rakhimov, J. Phys. D Appl. Phys. **50**(7), 075202 (2017), https://doi.org/10.1088/1361-6463/50/7/075202 .

[18] R. Ramos, G. Cunge, O. Joubert, N. Sadeghi, M. Mori, and L. Vallier, Thin Solid Films **515**(12), 4846–4852 (2007), https://doi.org/10.1016/j.tsf.2006.10.025.

[19] R.E. Walkup, K.L. Saenger, and G.S. Selwyn, J. Chem. Phys. **84**(5), 2668–2674 (1986), https://doi.org/10.1063/1.450339 .

[20] H.M. Katsch, A. Tewes, E. Quandt, A. Goehlich, T. Kawetzki, and H.F. Döbele, J. Appl. Phys. **88**(11), 6232–6238 (2000), https://doi.org/10.1063/1.1315332 .

[21] J.W. Coburn, and M. Chen, J. Appl. Phys. **51**(6), 3134–3136 (1980), https://doi.org/10.1063/1.328060 .

[22] S.-B. Lee, J.-H. Kim, G. Kim, J.-W. Park, B.-K. Chae, and H.-H. Choe, Applied Science and Convergence Technology **32**(5), 122–126 (2023), https://doi.org/10.5757/ASCT.2023.32.5.122 .

[23] Y.-H. Wang, L. Wei, Y.-R. Zhang, and Y.-N. Wang, Chinese Phys. B **24**(9), 095203 (2015).

[24] X.-Q. Zhao, Y.-S. Liang, and Y.-Y. Guo, Phys Plasmas **29**(11), (2022), https://doi.org/10.1063/5.0098152 .

[25] C.-C. Hsu, M.A. Nierode, J.W. Coburn, and D.B. Graves, J. Phys. D Appl. Phys. **39**(15), 3272–3284 (2006), **DOI** 10.1088/0022-3727/39/15/009.

[26] T.R. Gengenbach, G.H. Major, M.R. Linford, and C.D. Easton, J. Vac. Sci. Technol. A **39**(1), 013204 (2021), https://doi.org/10.1116/6.0000682 .

[27] A. Fujimoto, Y. Yamada, M. Koinuma, and S. Sato, Anal. Chem. **88**(12), 6110–6114 (2016), https://doi.org/10.1021/acs.analchem.6b01327.

[28] A. Fuchs, J. Scherer, K. Jung, and H. Ehrhardt, Thin Solid Films **232**(1), 51–55 (1993), https://doi.org/10.1016/0040-6090(93)90761-D.

[29] D.F. Franceschini, Thin Films And Nanostructures, Vol. 30 (2002), pp. 217–276.

[30] S. Wang, Y. Dong, C. He, Y. Gao, N. Jia, Z. Chen, and W. Song, RSC Adv. **7**(84), 53643–53652 (2017), DOI: 10.1039/C7RA10505C.

[31] G. Cunge, M. Darnon, J. Dubois, P. Bézard, O. Mourey, C. Petit-Etienne, L. Vallier, E. Despiau-Pujo, and N. Sadeghi, Appl. Phys. Lett. **108**, 093109 (2016), https://doi.org/10.1063/1.4942892 .

[32] T. Aizawa, and T. Fukuda, Surf. Coat. Technol. **215**, 364–368 (2013), https://doi.org/10.1016/j.surfcoat.2012.07.095.

[33] O. Joubert, P. Paniez, J. Pelletier, and M. Pons, Appl. Phys. Lett. **58**(9), 959–961 (1991), https://doi.org/10.1063/1.104455 .

[34] Y.-R. Zhang, Z.-Z. Zhao, C. Xue, F. Gao, and Y.-N. Wang, J. Phys. D Appl. Phys. **52**(29), 295204 (2019), **DOI** 10.1088/1361-6463/ab1dd3.